Available online at www.sciencedirect.com
SCIENCE DIRECT®
Bioorganic & Medicinal Chemistry 14 (2006) 800–814
Bioorganic & Medicinal Chemistry

# The binding of DNA intercalating and non-intercalating compounds to A-form and protonated form of poly(rC)·poly(rG): Spectroscopic and viscometric study

Rangana Sinha, Md. Maidul Islam, Kakali Bhadra, Gopinatha Suresh Kumar,* Anamika Banerjee† and Motilal Maiti

*Biophysical Chemistry Laboratory, Indian Institute of Chemical Biology, Kolkata 700 032, India*

Received 29 June 2005; revised 31 August 2005; accepted 1 September 2005
Available online 3 October 2005

**Abstract**—Polymorphic RNA conformations may serve as potential targets for structure specific antiviral agents. As an initial step in the development of such drugs, the interaction of a wide variety of compounds which are characterized to bind to DNA through classical or partial intercalation or by mechanism of groove binding, with the A-form and the protonated form of poly(rC)·poly(rG), been evaluated by multifaceted spectroscopic and viscometric techniques. Results of this study suggest that (i) ethidium intercalates to the A-form of RNA, but does not intercalate to the protonated form, (ii) methylene blue intercalates to the protonated form of the RNA but does not intercalate to the A-form, (iii) actinomycin D does not bind to either conformations of the RNA, and (iv) berberine binds to the protonated form by partial intercalation process, while its binding to the A-form is very weak. The DNA groove binder distamycin A has much higher affinity to the protonated form of the RNA compared to the A-form and binds to both structures by non-intercalative mechanism. We conclude that the binding affinity characteristics of these DNA binding molecules to the RNA conformations are vastly different and may serve as data for the development of RNA based antiviral drugs.


## 1. Introduction

In recent years, there have been extensive studies on elucidating factors that govern the affinity and specificity of binding of many small molecules to DNA.[1,2] This has led to the discovery of a series of molecules that bind to DNA by different mechanisms and exert their biological activities. Among the different types of non-covalent DNA interacting small molecules, intercalating and groove binding molecules are important tools in molecular biology and many are clinically useful in the treatment of cancer.[3,4] Intercalators are typically planar fused aromatic cations that slide between the base pairs of DNA and effectively fill the space formed between base pairs when the helix is locally elongated and partially unwound. Molecules that bind in the minor groove on the other hand contain arc-shaped unfused aromatic systems with terminal base functions. Intercalated molecules interact with adjacent base pairs through van der Waals forces coupled with electrostatic stabilization, while the groove binding molecules form hydrogen bonds with base pairs. Our present knowledge on the molecular nature of these two common DNA binding modes is largely derived from detailed X-ray crystallographic and molecular modeling studies apart from extensive NMR and physicochemical data.[5–8] In contrast with DNA, relatively scanty high resolution conformational information on one hand and the complex structural diversity on the other hand have hindered the development of small molecules that can specifically target RNA molecules. Nevertheless, ever since the knowledge that several serious diseases are indeed caused by RNA viruses and after the emergence of RNA viruses like HIV, and Hepatitis C virus (HCV) particularly, there have been concerted efforts to develop new antiviral compounds that can specifically bind to RNA molecules.[9] A rational design of RNA binding compounds, however, requires a detailed understanding of their mode and mechanism of action. RNAs

*Keywords*: A-form RNA; Protonated form RNA; Intercalators; Groove binders; RNA–ligand interaction.
* Corresponding author. Tel: +91 33 2472 4049; fax: +91 33 2473 5197/ 2472 3967; e-mail: gskumar@iicb.res.in
† Present address: Department of Chemistry, The City University of New York, Hunter College, 695, Park Avenue, New York, NY 10021, USA.

0968-0896/$ - see front matter © 2005 Elsevier Ltd. All rights reserved.
doi:10.1016/j.bmc.2005.09.007

are versatile molecules that can fold into diverse structures and conformations, and these structures can serve as receptors for specific drug recognition sites.[10,11] Studies so far have identified different classes of RNA binding drugs. Among them, heterocyclic intercalating compounds, aromatic diamidines,[12] aminoglycoside antibiotics,[13,14] etc., are the most important. One approach in the development of RNA targeted drugs has been to study the interaction of already known DNA binding compounds that have been fairly well characterized to gather information as to how they can selectively recognize different RNA conformations. One of the earliest approaches in this direction has been that of Wilson and co-workers[15–18] who performed studies with a wide variety of DNA binding compounds with synthetic RNA molecules and correlated the RNA binding property of arylquinones and its HIV activity. Binding of DNA intercalators like ethidium,[19,20] methylene blue,[21,22] acridine orange,[23,24] sanguinarine,[25,26] berberine,[27,28] quinoxaline derivatives,[29] and groove binding molecules like DAPI,[17,30] Hoechst,[31] berenil,[32] etc., with few natural and synthetic single, and double stranded RNA polymers were also investigated. Studies of many of the DNA intercalating compounds were also investigated with RNA triplexes as part of antigene strategy to target specific molecules to control the gene expression.[33] Our interest toward the goal of developing RNA binding molecules has been to enhance the fundamental data base by studying the binding of some DNA intercalating and groove binding molecules with two conformations of the hitherto less investigated synthetic RNA poly(rC)·poly(rG) in the A-form and the protonated form. We have chosen ethidium bromide (EB), methylene blue (MB), actinomycin D (AMD), berberine (BER), and distamycin A (DA) as the ligands; the structures of these molecules are given in Figure 1. Structurally, the EB molecule is composed of the planar tricyclic phenanthridium ring and a secondary phenyl group perpendicular to the primary ring system. MB belongs to the phenothiazinium dye having planar conjugated system, while AMD has a planar phenoxazinone chromophore with two pentapeptide lactones. BER with its partial saturation in one of the rings is slightly buckled, while DA has an isohelical structure compatible to groove binding. EB, MB, and AMD are characterized to bind DNA through intercalative mode, while BER is a partial intercalator and DA is a classical groove binding molecule. Sequences of CG are important and have been found to abundantly occur in the genome of several RNA viruses. Structurally this RNA adopts an A-form conformation under physiological conditions that undergoes conformational changes under the influence of protonation.[25] At pH 4.3 it adopts a protonated structure that is significantly different from the canonical A-conformation. In this communication, we report the binding characteristics of the above-described DNA interacting compounds with the two aforesaid structures of poly(rC)·poly(rG) in order to gain insights into the binding aspects of these molecules to RNA conformations.

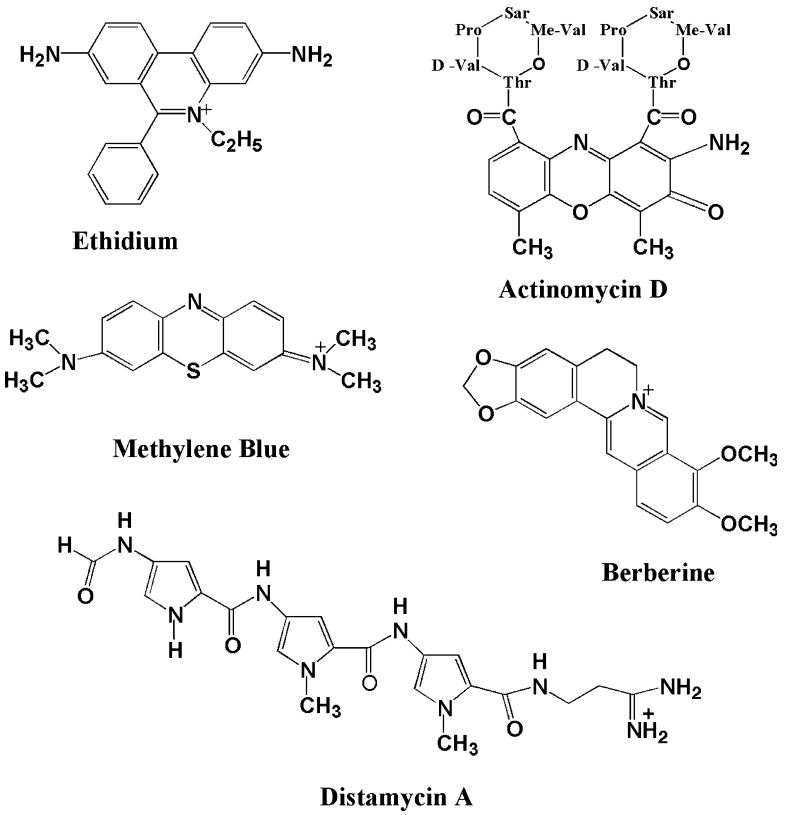


**Figure 1.** Chemical structures of ethidium, methylene blue, actinomycin D, berberine, and distamycin A.

## 2. Results

### 2.1. Spectral characteristics of the A-form and protonated form of poly(rC)·poly(rG)

The circular dichroic (CD) and absorption spectral characteristics of the double stranded poly(rC)·poly(rG) in the A-form and the protonated form are shown in Figure 2. At pH 7.0, the A-form structure of the RNA is characterized by a typical CD spectrum with a peak around 270 nm followed by a characteristic hump in the 255 nm region and a large negative peak the around 210 nm region (curve 1). On protonation, the positive peak ellipticity enhances and red shifts, while the hump slowly disappears. The protonated structure of the polymer at pH 4.3 has a CD spectrum (curve 2) with a higher ellipticity for the positive peak. The two spectra exhibited two isodichroic points at 238 and 264 nm, and observed in the series of spectra (not shown) undergoing pH-dependent transition.[25] The absorption spectral characteristics of these two structures are presented in the inset of Figure 2. At pH 7.0, the A-form structure has absorption maximum at 259 nm (curve 1, inset), while the protonated form exhibited peak at the same wavelength with lower molar extinction coefficient (curve 2, inset). A single sharp isosbestic point observed around 280 nm indicates the equilibrium between the two structural forms. This result is in conformity with our earlier observation.[25] It was also observed that both the UV and CD changes were completely reversible when the protonated polymer was transferred to neutral pH indicating the duplex nature of the protonated structure.

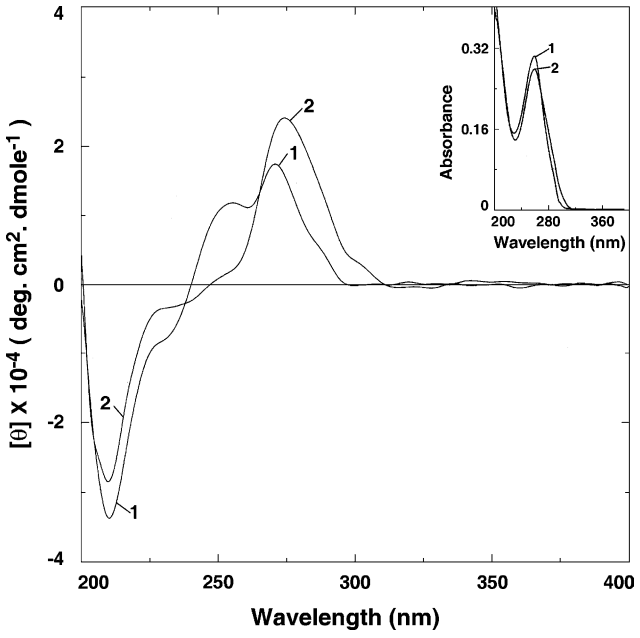


**Figure 2.** CD spectra of A-form (curve 1) and protonated form (curve 2) of poly(rC)·poly(rG) (45 μM) in 10 mM CP buffer, pH 7.0, and 4.3 at 20 °C, respectively. Inset: UV spectra of A-form (curve 1) and protonated form (curve 2) of 40.3 μM poly(rC)·poly(rG) under identical conditions.

Temperature dependent thermal melting studies on both A-form and protonated form indicated that the structures are thermally stable up to 99.5 °C and no strand separation was observed (not shown). Similarly in circular dichroic studies at different temperature, no conformational changes in the protonated structure were observed up to 50 °C.

### 2.2. Absorption spectral study

The effect of progressively increasing the concentration of A-form and protonated form of poly(rC)·poly(rG) on the absorption spectra of various ligands is presented in Figure 3. The characteristic hypochromism and bathochromism, and also sharp isosbestic points indicated clearly the equilibrium in binding phenomenon in all the cases, except for the A-form RNA–DA complex (Fig. 3G). The spectrum of EB in solution at both pH is identical with an absorbance maximum at 480 nm. In presence of either conformation of the RNA, hypochromicity changes and red shift of the wavelength maximum are observed (Fig. 3A and B). In the case A-form, a hypochromicity of about 48% and a bathochromic shift of about 20 nm were observed at the saturation *P*/*D* (nucleotide phosphate/drug molar ratio) of 24 with a sharp isosbestic point at 519 nm, while with the protonated form there were significantly large differences in both the hypochromism, bathochromism and the location of the isosbestic point at the saturation *P*/*D* of 48. The protonated form effected a hypochromic change of about 65% with a red shift of the wavelength maximum by 39 nm with the isosbestic point being centered around 522 nm.

The absorption spectral titration of MB with the two forms of the RNA is presented in Figure 3C and D. MB has an absorption spectrum with a wavelength maximum at 664 nm and is invariant with pH. Titration with the A-form polymer induces hypochromic effects and bathochromic shifts ($\Delta\lambda = 5.5$ nm) with the presence of an isosbestic point around 684 nm. With the protonated structure, MB spectra showed significantly larger hypochromic effects but lower bathochromic effects (Table 1).

BER, on the other hand, has two wavelength maxima in the visible region with a strong absorbance band with wavelength maximum around 344 nm and a weak but broad band around 420 nm. Berberine also does not exhibit any pH dependent absorbance changes in the pH range studied here. Both A-form and the protonated form of the RNA induced moderate hypochromic change and bathochromic shifts in the 344 nm and 420 nm peaks of the alkaloid with three characteristic isosbestic points centered around 357, 382, and 448 nm, respectively (Fig. 3E and F). But in this system also the wavelength shift and the percentage hypochromicity change at saturation were higher at 42% with the protonated form compared to the A-form at 33%.

DA has a single absorption peak around 303 nm that underwent continuous decrease on binding to the A-form with no saturation effects, while with the protonated form a hypochromic and bathochromic effect of the

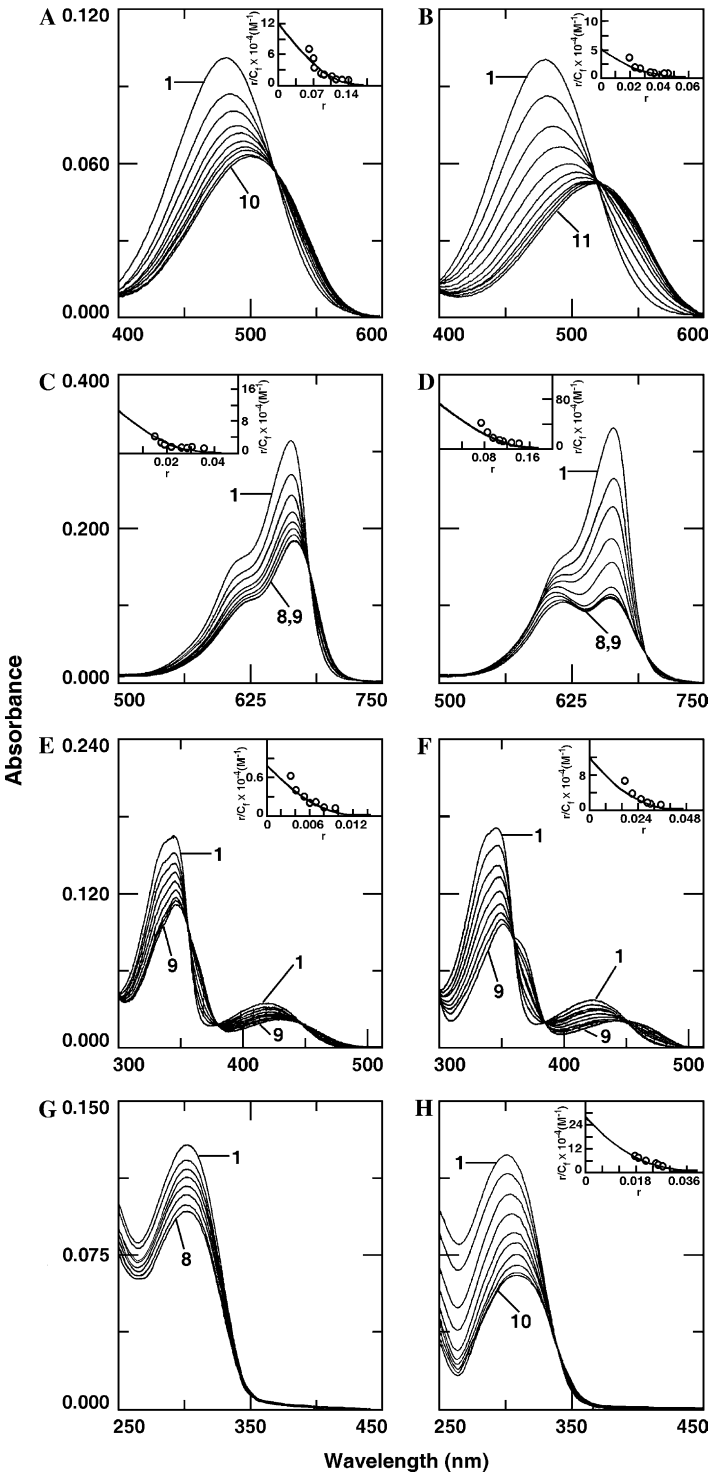


**Figure 3.** Representative absorption spectra in 10 mM CP buffer of (A) EB (17.70 μM) treated with 0, 47.26, 94.87, 141.60, 188.51, 235.23, 282.67, 325.86, 374.00, and 420.02 μM (curves 1–10) of A form of poly(rC)·poly(rG); (B) EB (17.50 μM) treated with 0, 87.38, 173.64, 259.64, 345.09, 430.01, 514.39, 598.24, 681.57, 764.38, and 846.68 μM (curves 1–11) of protonated form of poly(rC)·poly(rG); (C) MB (4.32 μM) treated with 0, 42.17, 84.00, 125.50, 156.33, 187.15, 227.83, 268.22, and 288.29 μM (curves 1–9) of A form of poly(rC)·poly(rG); (D) MB (4.44 μM) treated with 0, 8.88, 16.27, 26.64, 32.49, 48.66, 65.19, 80.84, and 96.85 μM (curves 1–9) of protonated form of poly(rC)·poly(rG); (E) BER (7.33 μM) treated with 0, 204.68, 406.9, 672.9, 1046.16, 1446.42, 1820.02, 2064.40, and 2305.15 μM (curves 1–9) of A form of poly(rC)·poly(rG); (F) BER (7.20 μM) treated with 0, 69.47, 138.67, 207.50, 276.24, 310.43, 344.62, 412.73, and 480.58 μM (curves 1–9) of protonated form of poly(rC)·poly(rG); (G) DA (3.43 μM) treated with 0, 36.98, 73.82, 110.51, 147.05, 183.45, 219.71, and 253.50 μM (curves 1–8) of A-form poly(rC)·poly(rG) (H) DA (3.40 μM) treated with 0, 23.35, 46.59, 69.71, 92.69, 115.64, 138.44, 161.13, 183.71, and 206.19 μM (curves 1–10) of protonated form of poly(rC)·poly(rG). All experiments were performed at 20 °C in, respective buffers. Inset: representative Scatchard plot of each complexation. The solid lines represent the non-linear least square best-fit of the experimental points to the neighbor exclusion model obtained using the computer programme SCATPLOT.[35] The best-fit data are in the range of 30% (lower limit) and 90% (upper limit). Values of '*K*' and '*n*' are presented in Table 3.

**Table 1.** Absorption and emission maxima and molar extinction coefficients of the drugs employed in this study

| Compounds | Absorption max $\lambda$ (nm) | Emission max $\lambda$ (nm) | $\varepsilon$ ($M^{-1}$ $cm^{-1}$) | Reference |
|---|---|---|---|---|
| Ethidium (EB) | 480 | 605 | 5680 | 54 |
| Actinomycin D (AMD) | 440 | 470 | 25,200 | 56 |
| Methylene blue (MB) | 664 | 685 | 76,000 | 22 |
| Berberine (BER) | 344 | 530 | 22,500 | 66 |
| Distamycin A (DA) | 303 | nf | 37,000 | 71 |

nf: non-fluorescent.

peak was observed with a sharp isosbestic point at 342 nm (Fig. 3G and H). The characteristic features of the wavelength maximum for each of these molecules and the data on their hypochromic and bathochromic behavior in the presence of either form of the RNA are presented in Table 2.

AMD has an absorption spectrum in the range 300–600 nm with a single wavelength maximum around 440 nm, the intensity of which decreased linearly with increasing concentration of both forms of RNA without achieving any saturation. No bathochromic effect or isosbestic points were observed in the series of spectra (not shown).

The presence of isosbestic points in the spectral titration enabled the calculation of the binding affinity of these molecules from absorption spectral changes in all cases, except for AMD and DA–A-form systems. The results of absorption spectral titration were converted to Scatchard plots (inset of Fig. 3). The binding isotherm in each case is non-linear and concave upward, suggesting the involvement of more than one type of binding site. Since we found no sign of sigmoidal behavior for the occurrence of cooperativity in our systems, we analyzed the data according to the neighbor exclusion model[34] using the SCATPLOT program[35] for non-cooperative binding phenomenon to fit our experimental data. Such a model has been observed to adequately fit our experimental data within the region of Scatchard plots corresponding to the range of 30% (lower) and 90% (upper) of each A-form and protonated form structure. The binding parameters of these compounds to the two forms of RNA are presented in Table 3. The data clearly reveal that the binding affinity of EB to A-form of the RNA is higher, while the affinity of MB to the protonated form is much higher in comparison with the A-form. The binding affinity of BER to the protonated form is higher compared to the same with the A-form, while DA also binds to the protonated form with higher affinity. Binding affinity of AMD to both the forms of RNA and DA to the A-form structure could not be ascertained due to the non-equilibrium in the binding process.

**Table 2.** Absorption spectral characteristics of various ligand interaction with A-form and protonated form of poly(rC)·poly(rG)[a]

| Compounds | A-form | | | | | Protonated form | | | | |
|---|---|---|---|---|---|---|---|---|---|---|
| | $\lambda_{initial}$ | $\lambda_{final}$ | $\Delta\lambda$ | Isosbestic points | % Hypochromicity | $\lambda_{initial}$ | $\lambda_{final}$ | $\Delta\lambda$ | Isosbestic points | % Hypochromicity |
| EB | 480 | 500 | 20 | 519 | 48 | 480 | 519 | 39 | 522 | 65 |
| AMD | 440 | 440 | nil | nil | ns | 440 | 440 | nil | nil | ns |
| MB | 664 | 670 | 6 | 684 | 43 | 664 | 664 | nil | 698 | 67 |
| BER | 344 | 347 | 3 | 357, 382, 448 | 33 | 344 | 350 | 6 | 357, 382, 448 | 42 |
| DA | 303 | 303 | nil | nil | ns | 303 | 313 | 10 | 342 | 52 |

ns: saturation could not be attained in these cases.

**Table 3.** Binding parameters for the interaction of EB, MB, BER, and DA with A-form and protonated from of poly(rC)·poly(rG) obtained form spectrophotometric and spectrofluorimetric analysis[a]

| Compound | Spectrophotometry | | | | Spectrofluorimetry | | | |
|---|---|---|---|---|---|---|---|---|
| | A-form[b] | | Protonated form[c] | | A-form | | Protonated form | |
| | $K\times10^4$ | $n$ | $K\times10^4$ | $n$ | $K\times10^4$ | $n$ | $K\times10^4$ | $n$ |
| EB | 12.0 | 5.8 | 5 | 17 | 11.0 | 6.5 | 3.2 | 26 |
| MB | 10.0 | 23 | 70 | 5.8 | 9.0 | 23.5 | 52 | 10 |
| BER | 0.8 | 70 | 12 | 21 | ns | — | 20 | 17 |
| DA | ns | — | 28 | 25 | nd | — | nd | — |

ns: saturation could not be attained in these cases.
nd as the sample is non-fluorescent.
[a] Average of four determinations in each case.
[b] In 10 mM citrate–phosphate buffer, pH 7.0.
[c] In 10 mM citrate–phosphate buffer, pH 4.3.

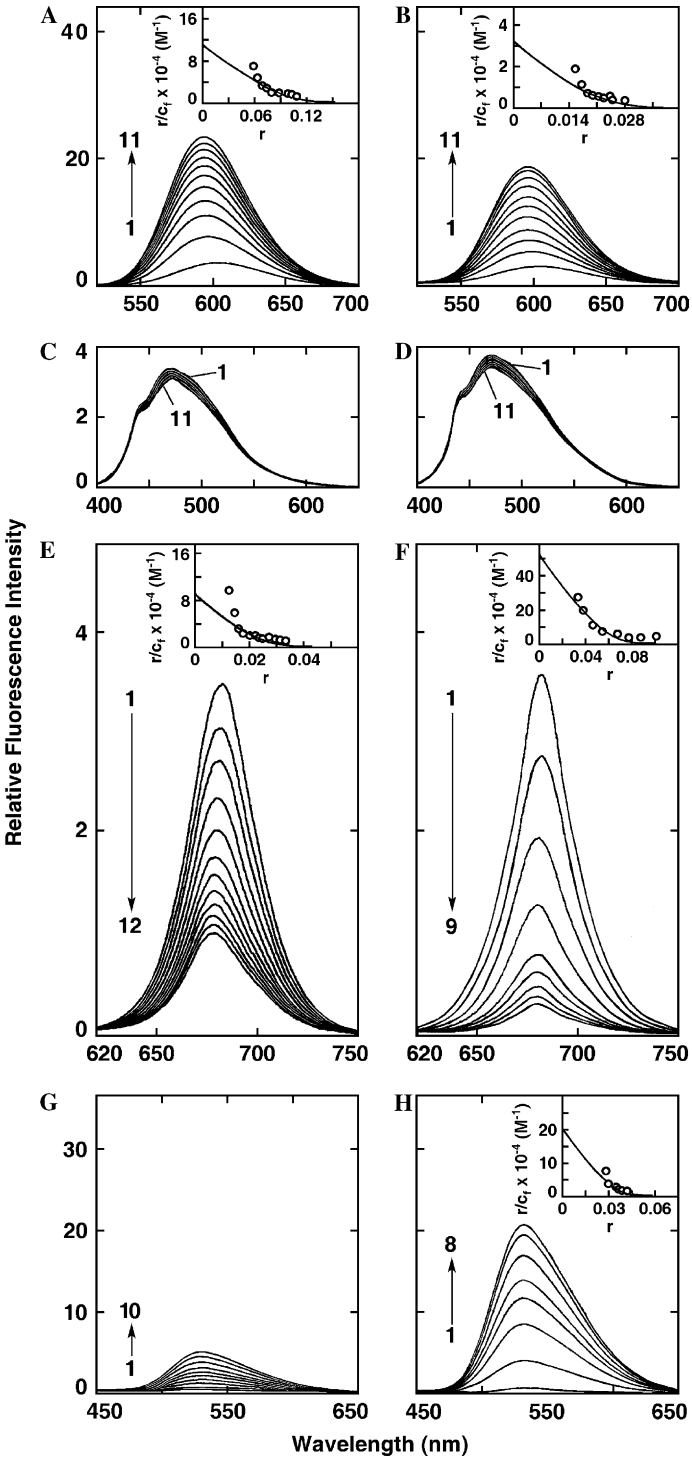


**Figure 4.** Representative steady state fluorescence emission spectrum in 10 mM CP buffer of (A) EB (9.65 μM, curve 1) treated with 18.15, 36.22, 54.22, 72.15, 90.01, 107.80, 125.52, 143.16, 160.74, and 178.25 μM (curves 2–11) of A form of poly(rC)·poly(rG); (B) EB (9.57 μM, curve 1) treated with 49.63, 99.25, 148.88, 210.91, 285.35, 359.79, 434.23, 508.67, 583.11, and 657.55 μM (curves 2–11) of protonated form of poly(rC)·poly(rG); (C) AMD (0.95 μM, curve 1) treated with 6.53, 13.04, 19.52, 25.97, 32.40, 38.81, 45.19, 51.54, 57.87, and 64.17 μM (curves 2–11) of A-form of poly(rC)·poly(rG); (D) AMD (0.95 μM, curve 1) treated with 6.55, 13.09, 19.64, 26.18, 32.73, 39.27, 45.82, 52.36, 58.91, and 65.45 μM (curves 2–11) of protonated form of poly(rC)·poly(rG); (E) MB (4.78 μM, curve 1) treated with 24.10, 48.13, 80.05, 119.78, 159.32, 198.65, 237.80, 276.65, 315.51, 354.08, and 392.46 μM (curves 2–12) of A form of poly(rC)·poly(rG); (F) MB (4.78 μM, curve 1) treated with 16.09, 40.23, 64.36, 96.55, 136.77, 185.05, 241.36, and 321.82 μM (curves 2–9) of protonated form of poly(rC)·poly(rG); (G) BER (9.80 μM, curve 1) treated with 53.64, 142.76, 231.52, 319.94, 408.01, 495.72, 617.94, 739.49, and 843.15 μM (curves 2–10) of A-form of poly(rC)·poly(rG); (H) BER (9.57 μM, curve 1) treated with 67.70, 108.20, 135.13, 175.46, 215.70, 242.41, and 269.20 μM (curves 2–8) of protonated form of poly(rC)·poly(rG). All experiments were done in 10 mM CP buffer of pH 7.0 for A-form and pH 4.3 for protonated form at 20 °C. Inset: representative Scatchard plot of each complexation. The solid lines represent the non-linear- least-squares best-fit of the experimental points to the neighbor exclusion model obtained using the computer program SCATPLOT.[35] The best-fit data are in the range of 30% (lower limit) and 90% (upper limit). Values of '*K*' and '*n*' are presented in Table 3.

### 2.3. Fluorescence spectral study

The binding of the fluorescent compounds, EB, AMD, MB, and BER, to the A-form and the protonated form of poly(rC)·poly(rG) structures was studied by spectrofluorimetry. The result of such study is presented in Figure 4. EB has a very strong fluorescence spectrum in the 520–700 nm region with an emission maximum at 605 nm when excited at 510 nm. With increasing concentrations of either form of RNA, a progressive enhancement of fluorescence intensity was observed until saturation was reached (Fig. 4A and B). In both the cases, a gradual blue shift in the emission peak maximum was observed as the binding progressed. At saturation, the A-form RNA–EB complex had a slightly higher fluorescence intensity but at a lower *P*/*D* ratio compared to the protonated form–EB complex; but the band maximum in both cases was located at around 595 nm.

AMD has a weak fluorescence in aqueous buffers with an emission maximum around 470 nm when excited at 390 nm. Figures 4C and D show that with increasing concentrations of either A-form or protonated form of poly(rC)·poly(rG) no significant change in the fluorescent spectral patterns was observed.

MB has fluorescence emission in the 620–750 nm region with emission maximum at 685 nm on excitation at 610 nm. It does not show any pH dependent fluorescence properties. In presence of both the A-form and the protonated form of the RNA, progressive quenching of the MB fluorescence was observed (Fig. 4E and F). Saturation was achieved at a *P*/*D* of 82 in the MB–A-form fluorescence, while in the case of MB-protonated form it was achieved at a *P*/*D* of around 65. Complexation with both structures blue shifted the emission maximum of MB fluorescence by about 3 nm. Further, the residual fluorescence of the saturated A-form–MB complex was significantly higher than that of the protonated complex.

In aqueous buffers at both pH 7.0 and 4.3, BER has a very weak fluorescence that gives an emission spectrum in the region 450–650 nm with a maximum at 530 nm when excited at 350 nm. Binding to both A-form and the protonated form of the RNA polymer enhanced the fluorescence intensity of berberine (Fig. 4G and H) with negligible shift in the emission maximum. It can be seen that the enhancement of fluorescence of binding of BER was much higher with the protonated form compared to the A-form, suggesting clear differences in the nature of orientation or environment of bound BER molecules on these structures.

The results of fluorescence titration data were also converted to Scatchard plots that were further analyzed according to an excluded site model[34] using SCATPLOT program[35] for non-cooperative binding phenomenon to fit our experimental data. The binding isotherm of each system obtained from the fluorimetric data is illustrated in the inset of Figure 4. The data of '*K*' and '*n*' obtained from the analysis of the Scatchard plots are also presented in Table 3.

### 2.4. Quantum yield

The quantitative data on fluorescence quantum yield of EB, MB, and BER complexes with the A-form and the protonated form of poly(rC)·poly(rG) are depicted in Figure 5A and B, respectively. It can be seen that with the A-form, the relative quantum yield of EB enhances and levels off at saturation. The $\phi/\phi_0$ for MB–A-form decreases with increasing *P*/*D* values until saturation is reached. On the other hand, with the protonated form, the $\phi/\phi_0$ values of EB and BER increased with the *P*/*D*, the latter to a larger extent until saturation was achieved, while for MB, the decrease in $\phi/\phi_0$ value was more pronounced (Fig. 5B) compared to the A-form.

### 2.5. Fluorescence polarization anisotropy

Fluorescence polarization anisotropy (FPA) measurements also provide evidences for the binding of these molecules to the A-form and protonated form structures. It has been found that the fluorescence polarization upon binding of EB to the A-form of RNA shows a value of 0.2 at saturation against a value of 0.03 for free EB under identical condition. A similar FPA value is obtained for protonated form RNA–MB complex. The FPA value of berberine complexation to both the A-form and the protonated form of RNA was significantly lower, indicating that BER has weak binding to both the structures of the RNA.

### 2.6. Circular dichroism

Circular dichroic spectral studies of the A-form and protonated form of the RNA in the spectral region 210–400 nm were employed to monitor the drug induced conformational changes of the host nucleic acid structure. Figure 6 shows the intrinsic CD spectral changes of the A-form and protonated form of the RNA on the interaction with several ligands. The characteristic A-form and protonated form spectra of poly(rC)·poly(rG) undergo CD spectral changes in presence of each of the ligands with either increase or decrease in molar

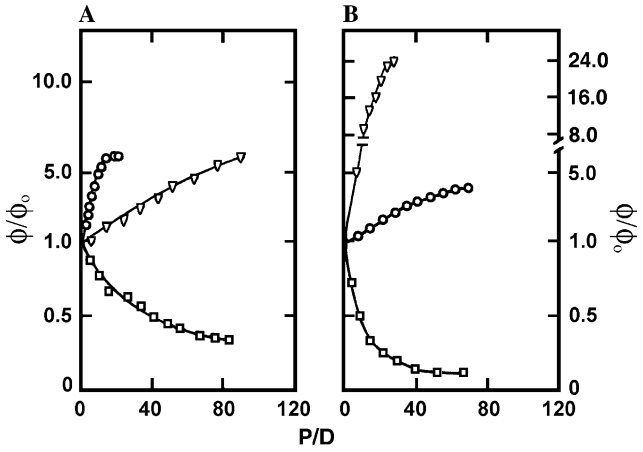


**Figure 5.** Plots of the relative quantum yield $\phi/\phi_0$ versus *P*/*D* for interaction of EB (○–○); MB (□–□); BER (▽-▽) with A-form (A) and protonated form (B) of poly(rC)·poly(rG).

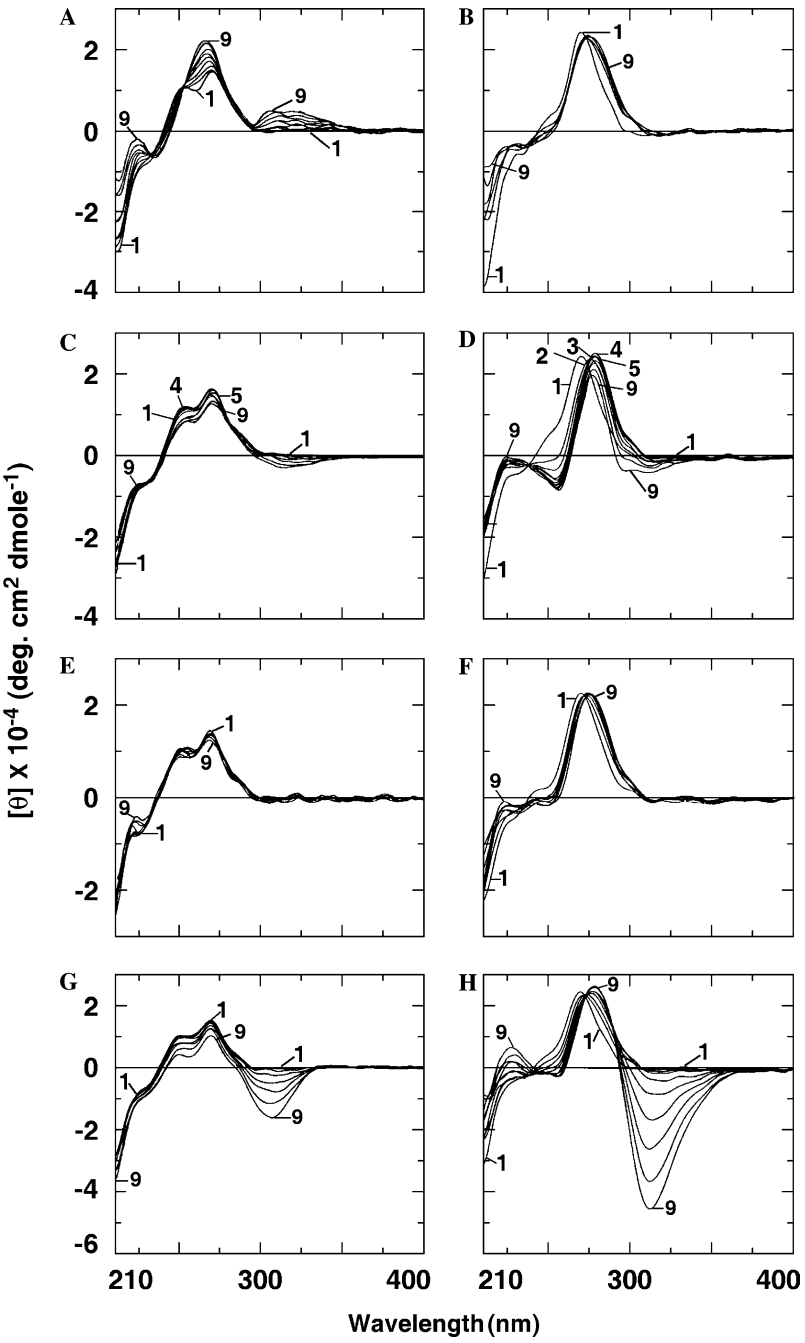


**Figure 6.** Representative CD spectra resulting from the interaction of various drugs with A-form (panels A, C, E, and G) and protonated form (panels B, D, F, and H) of poly(rC)·poly(rG) (30.04 μM) in 10 mM CP buffer of pH 7.0 or 4.3 at 20 °C. Curves (1–9) in each complex denote 0, 3.00, 6.01, 9.01, 12.02, 15.02, 18.02, 21.03, and 24.03 μM EB (panels A and B), MB (panels C and D), BER (panels E and F), and DA (panels G and H) for the complexation with A-form and with protonated form, respectively. The expressed molar ellipticity is based on the RNA concentration.

ellipticity value with increasing concentrations of each ligand shift of the band maximum of the 270 nm band followed by further marginal changes. In case of EB, the A-form spectrum (Fig. 6A) undergoes enhancement in the 270 nm positive peak that eventually reached saturation. Two isoelliptic points centered around 232 nm and 254 nm characterize the interaction and this also implies that a single type of drug complex is formed in this system. Concomitant with the CD changes there was the development of a strong induced CD band for the bound EB molecules in the 320 nm region. On the other hand, the changes with the protonated form showed an initial red shift of the band maxima of the 270 nm band followed by further marginal changes on further binding. But the negative band ellipticity showed reduction in its intensity as the binding progressed. It is significant to note that in this case no induced CD band was developed for the bound EB in the 320 nm region.

The CD spectral data on the interaction of MB with the two forms of RNA are presented in Figure 6C and D. With the A-form, there was a small decrease in the positive peak with the concomitant development of a small negative induced CD in the 320 nm region for bound

MB molecules. With the protonated form, there was an initial red shift of the positive band maximum followed by a decrease in the peak intensity on further binding of MB molecules. A sharp negative extrinsic CD band also is apparent here in the 300–330 nm region.

The binding of BER to the A-form resulted in only marginal changes in the CD spectra (Fig. 6E), while the protonated form showed a small red shift and further enhancement in the intensity of the peak (Fig. 6F).

The CD spectral changes on the interaction of DA with the two conformations of poly(rC)·poly(rG) are depicted in Figure 6G and H, respectively. With the A-form, a decrease in the peak ellipticity was apparent with the concomitant formation of a negative extrinsic CD band around 310 nm that increased in intensity as the binding progressed. With the protonated form, the CD changes showed gradual red shift and enhancement in ellipticity with an isoelliptic point around 275 nm. The development of large negative CD in the 310 nm for the bound DA molecules characterizes the strong binding of DA to the protonated conformation of the RNA.

The binding of AMD was also studied by similarly monitoring circular dichroic changes. It was found that AMD did not perturb the CD spectra of either form of the RNA.

### 2.7. Viscometric titrations

The viscometric technique is a well-established method for investigating the extension of DNA or RNA helix associated with intercalation. The effect of these ligands on the viscosity of linear rod-like RNA duplex in both A and protonated forms was studied. The relative length increase ($L/L_o$) against $r$ was dependent on $r_{max}$ of each complex (not shown). The extent of length enhancement of the A-form or protonated form of the RNA duplex was estimated with respect to a standard value of $\beta = 2$ corresponding to a length enhancement of 0.34 nm. The $\beta$ values for EB-A-form poly(rC)·poly(rG) and MB-protonated form poly(rC)·poly(rG) systems showed values 1.95 and 1.86, respectively. Again, in case of DA-protonated form system, considerable enhancement of the helix was observed with a $\beta$ value of around 1.12. Binding of MB to the A-form, and BER to the protonated form of the RNA caused small changes in the $\beta$ values, while no appreciable viscosity changes were observed on EB binding to protonated form, and BER and DA binding to the A-form of the RNA. Table 4 illustrates the $\beta$ values, the helix length enhancement ($\Delta L$), and the percentage of helix length increment at $r_{max}$ ($L_p$, %) for the binding of these molecules to A-form and protonated form of the RNA polymer.

## 3. Discussion

Although intercalation and minor groove binding modes of several organic molecules with B-form DNA have been well documented, less study is available on similar complexes with RNA. In order to strengthen this area of research and with the long range objective of developing drugs that can selectively target RNA, we have studied the interaction of five DNA binding molecules with two different conformations of poly(rC)·poly(rG) structures. poly(rC)·poly(rG) has been previously shown[25] from our laboratory to exist in two conformations depending on the pH of the solution; the A-form at physiological pH and the protonated form at pH 4.3. These two conformations have been characterized to have clearly defined but distinctly different CD and UV spectral characteristics. But none of these forms exhibited any thermal melting profiles within 99.5 °C, indicating that both these structures are thermally stable up to a temperature of 99.5 °C under the conditions of our study. Protonation of nucleic acid bases could result in base pair reorientation that could lead to structural alterations. Although there is consensus that the first protonation sites in DNA are the GC base pairs, there is still controversy as to whether the guanines or the cytosines are protonated first. Based on the fact that cytosine possesses the highest pK amongst the four bases, earlier studies led to the suggestion that the N3 of cytosine is the initial site of protonation.[36] Contrary to this, Guschulbauer and Courtois[37] proposed the initial protonation sites to be the N7 of guanine. This would result in an interesting consequence resulting in the subsequent swinging around of a GC base pair to *syn* conformation and sharing the protons with the N3 of cytosine. It was argued that the N7 of guanines lie in the major groove and is thus easily accessible to protons, while the N3 of cytosine is involved in base pair hydrogen bonding. Later studies using

**Table 4.** Viscometric properties of the binding of the ligands with A-form and protonated form of poly(rC)·poly(rG)[a]

| Compound | A-form | | | Protonated form | | |
|---|---|---|---|---|---|---|
| | $\beta$ | $L$ (nm)[b] | $L_p$[c] (%) | $\beta$ | $L$ (nm) | $L_p$ (%) |
| EB | 1.95 | 0.33 | 19.5 | nd | nd | nd |
| MB | 1.01 | 0.17 | 3.0 | 1.86 | 0.32 | 19.0 |
| BER | nd | nd | nd | 0.76 | 0.13 | 2.5 |
| DA | nd | nd | nd | 1.12 | 0.19 | 12.0 |

nd: not detected as the specific viscosity enhancement is very low in each case.

[a] Data presented from the average of five determinations in each case.

[b] Length enhancement per intercalation site, $L = 0.34$ nm corresponds to the standard value of $\beta = 2$.

[c] Percent helix length enhancement at $r_{max}$ of each polymer ($L_p$, %). Relative length enhancement ($\Delta L/L_o$) is given by $\Delta L/L_o = \beta r$ and hence $L_p$ is calculated from $(\Delta L_{max}/L_o) \times 100 = \beta r_{max} \times 100$.

NMR[38,39] have however supported the former model of initial cytosine protonation. Studies from our laboratory[40–42] on protonation of natural DNAs and synthetic alternating GC polymer have proposed specific conformational changes to left-handed structures that resulted from Hoogsteen base pairing formation in the GC pairs. But in the DNA GC homopolymer, such left-handed conformation with Hoogsteen base pairing was not formed.[42] Studies on the protonated structures of RNA polymers are still scanty. Poly(rC) and poly(rG) have been associated at low pH to form poly ($rC^+$)·poly (rG)·poly(rC) triplex with the poly (rC) strand lying in the major groove. Similarly, acid titration of poly(rC)·poly(rG) duplex has been suggested to lead to triplex formation.[43] Single stranded ribonucleic acids of poly(rG) and poly(rC) have also been reported to form alternate structures under protonation like double stranded and quadruplex structures.[44] Protonation of single stranded poly(rA) would result in the formation of a parallel stranded duplex structure resulting from the base pairing of protonated adenine residues.[45] In the RNA homopolymer of GC studied here, protonation resulted in the formation of a duplex structure having clearly different CD and UV characteristics compared to its A-form. But from thermal melting studies, we found no evidence for the formation of Hoogsteen base pairing in this conformation at pH 4.3 with which studies on the interaction of the drugs were performed.

### 3.1. Ethidium–RNA interaction

Ethidium bromide (EB) is a phenanthrinic drug that forms soluble metachromatic complexes with nucleic acids. The molecule also was reported to have potent antiviral activity and has the ability to inhibit retroviral reverse transcription.[46] The mechanism of EB–nucleic acid interaction, particularly with DNA, has been extensively studied and it has been consensually proposed that EB binds primarily to DNA by classical intercalation mode,[47] while secondary binding could occur by a stacking mechanism. Our studies indicate hypochromic and bathochromic effects on the absorption band of ethidium on addition of both A-form and protonated form structures, but the changes were more rapidly pronounced in the A-form structure. Similarly, the enhancement of the fluorescence although pronounced in both cases, the changes were more rapid and achieved saturation at lower *P*/*D* values with the A-form structure when compared with the protonated form. The binding data derived in terms of affinity and the excluded sites from both the spectrofluorimetric and spectrophotometric data again substantiate that EB strongly binds to the A-form of RNA polymer. We have obtained binding affinity values of $12 \times 10^4\ M^{-1}$ and $11 \times 10^4\ M^{-1}$, respectively, by spectrophotometric and spectrofluorimetric experiments for the binding of EB to the A-form RNA while the same for the protonated form was much lower (Table 3). Previous studies by Quadrifoglio and colleagues[19] have evaluated a binding constant of $0.8 \times 10^3\ M^{-1}$ for EB binding to A-form of poly(rC)·poly(rG) at 100 mM [$Na^+$]. Bresslof and Crothers[20] studied the binding of EB to several synthetic RNA and RNA–DNA hybrids and reported a higher binding affinity for EB to RNA and RNA hybrids relative to DNA in the poly[AU(T)] series. Nelson and Tinoco[48] in oligonucleotides and Baguli and Falkenhaug[49] in synthetic polynucleotides also observed higher binding affinity of EB to AU sequences of RNA. Crystal structures of EB intercalated complex in both DNA and RNA have similar geometries. Our data reveal that the binding of EB to the A-form of RNA is stronger than that to the protonated form. This has been further substantiated from the quantum yield data of EB-A-form system that was higher and achieving saturation more rapidly at lower *P*/*D* values compared to that with the protonated form. In CD, changes in the intrinsic CD of the polymer and the emergence of extrinsic CD for the bound EB molecules (Fig. 6A) when compared to lower changes with the protonated form and the total absence of extrinsic CD bands with the protonated system again underscore the intercalative binding of EB to the A-form structure of poly(rC)·poly(rG). The typical induced CD bands with low amplitude similar to that seen here (Fig. 6A) with the A-form RNA were suggested to be the result of direct interaction of EB molecules bound intercalated in neighboring binding sites.[50] Binding of EB to ribosomal RNA by spectroscopic techniques has suggested the intercalation of the phenanthridinium ring in the double stranded regions of RNA resulting in increased dye–dye interactions compared to DNA.[51] EB was also shown to intercalate to the A-form alternating GC RNA, but did not have any affinity with the Z-form of the same polymer.[52] In this context, it is worth noting that EB has been shown to convert all altered forms of DNA like Z-form, $H^L$-form, etc., back to the B-form.[53,54] In our studies, the diagnostic proof of intercalation came from the viscosity data (Table 4) which clearly showed that the viscosity of the rod like A-form RNA only has been enhanced by the intercalation of EB resulting in a helix extension value ($\beta$) of 1.95 in agreement with the previous results,[19,20] while none or only marginal changes were observed with the protonated form. Thus, from the data on EB, it is clear that EB binds to the A-form RNA by intercalative binding, while with the protonated form only either external and/or stacking interaction is revealed.

### 3.2. Actinomycin D–RNA interaction

Actinomycin D is one of the best-known and most widely used antibiotics. AMD is an antitumor agent, specific inhibitor that specifically inhibits the elongation phase of transcription. The mode of action of the drug is associated with binding to DNA that occurs by intercalation with its cyclic pentapeptide rings snugly fitting into the minor groove of DNA. The structure of AMD–DNA complex has been examined at the nucleotide level by different methods such as chemical footprinting, NMR, and X-ray crystallography.[55] AMD and several of its derivatives have also been shown to bind with high affinity to selected single stranded DNA, single stranded RNA, poly(I), but with low affinity to poly(dG) and r-RNA.[56] Our present results indicate that the binding of AMD to both the forms of RNA is non-specific as revealed from the results of UV titration, absence of changes in the fluorescence, and CD spectra and above all no enhancement in the viscosity of the rod like RNA.

### 3.3. Methylene blue–RNA interaction

Methylene blue is a polyaromatic cationic dye of the phenothiazine group used in staining of nucleic acids. MB has been shown to inactivate viruses in human plasma on exposure to light.[57] MB is an extensively used photosensitizing agent for photodynamic inactivation of RNA viruses including HIV, hepatitis B, virus and hepatitis C virus in plasma.[58] Very recently, inactivation of dengue virus by MB/narrow bandwidth light system has been reported.[59] Most biophysical studies on the interaction of MB with nucleic acids were performed with DNA.[60,61] MB has been shown to bind to DNA predominantly in intercalative mode with a 100-fold higher GC base pair specificity compared to AT base pairs. MB has also a weak affinity mostly due to electrostatic interaction to single stranded DNA, poly(rA) and poly(rG).[62] Binding of MB to t-RNA was shown to have pronounced effect on the aminoacylation activity.[63] The interaction of MB with A-form and protonated form of the RNA studied here indicated that the effect on the protonated form was more drastically pronounced in both absorbance and fluorescence compared to the A-form. In absorbance, more hypochromic effects of the visible absorption bands were manifested in presence of the protonated form (Table 2). Again, in fluorescence a more effective quenching of the intrinsic MB fluorescence was effected by the protonated form of the RNA rather than the A-form. Significantly, while DNA has been shown to cause red shift in the fluorescence of MB,[64] with RNA here we find a blue shift in the MB fluorescence spectrum. The binding parameters obtained from both absorbance and fluorescence experiments further revealed a stronger binding of MB molecules to the protonated conformation (Table 3). The data of binding affinity of MB to protonated form obtained from absorbance and fluorescence spectral data were about seven and five times higher than that with the A-form under identical conditions. In CD, more pronounced changes were achieved within the protonated form-MB system in terms of the perturbations in the RNA structure. Furthermore, the extrinsic CD of the bound MB molecules arising out of the coupling of the ligand transitions with RNA bases were more effective in the protonated form as evidenced by larger ellipticity values. Similar extrinsic CD was also reported on the binding of MB to t-RNA.[21] Viscosity experiments showed that the relative specific viscosity of the rod like protonated form RNA molecules was enhanced more effectively on binding to MB, the $\beta$ value was found to be 1.86 against a value of 1.01 with the A-form establishing that MB molecules bound to the protonated form by intercalative mechanism. Spectroscopic studies also indicated that MB can intercalate to t-RNA and partially intercalate to poly(rA) chains.[21,22] Intercalation of MB to double stranded RNA has been shown to mediate RNA–protein cross-links by MB molecules.[65]

### 3.4. Berberine–RNA interaction

Berberine is an isoquinoline plant alkaloid that partially intercalates to DNA.[66,67] Previous studies form our laboratory have shown that the alkaloid has a higher affinity for single stranded poly(rA) chains, compared to DNA, t-RNA, and several other single stranded synthetic RNA molecules.[27] The binding affinity of this alkaloid to both the conformations of RNA has been weak in comparison to MB or EB. Between the two conformations, the binding to the protonated form has been higher than that with the A-conformation. This has been substantiated from the results of absorbance and fluorescence studies. The binding data both from absorbance and fluorescence data showed higher binding affinity of the alkaloid to the protonated form. The circular dichroic change however does not indicate any major structural changes in the structure of the RNA conformations on binding of berberine. The binding mode determination by viscosity studies revealed that berberine does not intercalate into the A-form or protonated form of the RNA. With the protonated form a $\beta$ value of 0.76 was observed (Table 3) signifying a weak and partial intercalation of berberine molecules to the protonated structure.

### 3.5. Distamycin A–RNA interaction

Distamycin A is one of the best-known antiviral antibiotics that binds to double stranded DNA in the minor groove by replacing the spine of hydration and strongly favoring AT rich regions as its binding site. The crystal structure of DA with oligonucleotides has clearly elucidated the specificity of DA to AT sequences in the minor groove of DNA.[68] Not many studies however, are available on the nature of interaction of this molecule with RNA. Recently, the binding of DA and some of its derivatives with structured RNA of HIV-1 TAR RNA reported that DA by itself was ineffective in binding to RNA.[69] On binding to RNA in the A-form, there was only a hypochromic shift with no evidence of bathochromism or isosbestic points. In this circumstances, attempts to determine a binding constant for DA–A-form poly(rC)·poly(rG) were unsuccessful. Thus, the DA–A-form RNA could not be properly quantified. The circular dichroic spectral data nevertheless appear to favor an interaction of DA with the A-form structure with the formation of an extrinsic CD band in the 310 nm for the bound DA molecules. The binding of DA to DNA has been known to generate positive extrinsic CD in the 340 nm region. Note, however, that the extrinsic CD observed in the case of RNA is negative in magnitude and centered around 310 nm.[70] Viscosity studies indicated a small increment of the relative viscosity. A remarkably different picture was apparent for the interaction of DA with the protonated form of RNA. We found a hypochromic and bathochromic shift in the absorption band of the DA molecules in presence of increasing concentration of the protonated form with a single sharp isosbestic point around 342 nm showing equilibrium between bound and free DA molecules. This enabled the quantification of the binding and the Scatchard binding isotherm indicated non-cooperative binding phenomenon yielding as association constant ($K$) of $2.8 \times 10^5\ M^{-1}$ (Table 3). This value is comparable to a value of $5.7 \times 10^5\ M^{-1}$ reported by Waring and coworkers[71] for DA binding to CT DNA under similar conditions. Viscosity studies show that $\beta$ value is 1.12

with protonated form RNA on interaction of DA, indicating that it binds to this structure in a non-intercalative manner. However, electric linear dichroism studies with classical minor groove binding ligands like Hoechst 33258, berenil, and DAPI with TAR RNA have suggested the involvement of intercalation to the A-form RNA.[72]

## 4. Conclusions

The results presented in this paper on the interaction of several DNA binding molecules to two conformations of the synthetic RNA advance several new information regarding the RNA binding aspects of these molecules. Results from spectrophotometric, spectrofluorimetric, circular dichroism, and viscosity experiments indicate that (i) binding of EB to A-from RNA proceeds by intercalation similar to that observed for DNAs. It appears that the intercalated geometry of the EB molecules on the A-form RNA is similar to the DNA intercalation sites. This result is in agreement with the binding of EB to several other RNA models.[30] EB, on the other hand binds weakly with the protonated form, the structure of which is conformationally different from that of the A-form. (ii) MB molecules bind to the protonated form by intercalation, but its binding to A-form structure is presumably by some other mechanism which could not be established from the present study. The binding affinity is higher with the protonated form than the A-form structure. (iii) AMD–RNA interaction data reveal that this molecule does not bind to both the conformations of RNA. (iv) The partial intercalator BER binds to both A-and protonated form relatively weakly and apparently weaker than its binding to DNA, (v) The DNA groove binder DA on the other hand binds strongly in the minor groove of the protonated forms, while the binding to the A-form is also in the minor groove and is electrostatic in nature. The binding to the protonated form of CG sequences may be more facilitated in the absence of steric hindrance by the 2-$NH_2$ group of guanine. In contrast to DNA, the minor groove of A-form RNA has significantly different characteristics in terms of steric and chemical characteristics being more shallow, wide, and electrostatically positive and due to features such as the 2′-OH group in the RNA minor groove and the different relative molecular potentials.[73] The protonated form of the RNA may further differ from the A-form due to the protonation of the guanine and cytosine bases. X-ray diffraction data on the intercalation complexes of dinucleotides and modeling studies with intercalators in segments of RNA and DNA have indicated similar geometry of the intercalation sites in A-form RNA and B-form DNA.[74] At present, our data cannot differentiate the different geometries of the binding of the molecules studied here with A-form and protonated RNA, but it appears that the molecular disposition of the sites in these two conformations is quite different as being probed by both intercalators and groove binders. EB, MB, and BER are structurally different: EB has a planar structure with a phenolic group attached; MB is planar and linear, while BER with its partial saturation in one of the ring has a slightly buckled structure. Further, the minor and major grooves of the protonated structure of poly(rC)·poly(rG) are significantly different from that of its A-form. Binding of these drugs to the two forms of the RNA depends on the electrostatic interaction as well as their acceptability to the geometry of the minor groove for intercalation or partial intercalation. The relatively higher affinity of cationic MB and BER to the protonated form in comparison to the A-form of the RNA observed here is due to the higher adaptability in the minor groove of the protonated structure. Thus, depending on the structure of these ligands and local variations in the conformation, binding may be stronger to protonated RNA than A-form RNA. To conclude, from the standpoint of the design of potential RNA targeted drugs, and the diverse conformational variations possible for the RNA, our data present significant insights into the nature of binding of these DNA binding molecules to two forms of RNA helix.

## 5. Materials and methods

Poly(rC)·poly(rG) was purchased from Sigma Chemical Co., St. Louis, MO, USA, and was checked for its purity and nativeness before use. The concentration of this polymer was estimated spectrophotometrically using a molar extinction coefficient ($\varepsilon$) of 7700 $M^{-1}$ $cm^{-1}$ at 259 nm in buffer of neutral pH.[25] EB, AMD, BER, and DA were products of Sigma Chemical Company (St. Louis, MO, USA). MB was from Qualigens (India). The molar extinction coefficients of these compounds and their optical properties are collated in Table 1. The purity of these compounds was confirmed by thin layer chromatography, melting point determination, UV–vis spectroscopy, and $^1H$ NMR. Drug solutions were prepared freshly each day by dissolving appropriate amount in buffer of pH 7.0 and were always kept protected in dark to prevent from any light induced changes. All these compounds obeyed Beer's law in the concentration range used here. Studies were carried out in citrate–phosphate (CP) buffer containing 5 mM $Na_2HPO_4$·2-$H_2O$ as described previously.[40–42] The pH was adjusted by the addition of citric acid. This buffer provides constant [$Na^+$] molarity of 10 mM. Analytical grade reagents and glass distilled deionized water were used throughout. All the buffer solutions were passed through Millipore filters of 0.45 μm.

### 5.1. Formation of protonated structure of poly(rC)·poly(rG)

Protonated form of the RNA was prepared by slowly adding the A-form structure to CP buffer of pH 4.3 under stirring maintained at 15 °C. The formation of the structure was confirmed by CD measurements before further study. Although the formation of the structure appeared to follow fast kinetics, as revealed from CD, in practice a 30 min incubation time was allowed for the stabilization of the protonated structure before further measurements.

### 5.2. Absorption and fluorescence spectroscopy

All Absorbance and fluorescence measurements were recorded with a Shimadzu Pharmaspec 1700 spectrophotometer (Shimadzu Corporation, Japan) and a Hitachi F 4010 spectrofluorimeter (Hitachi Ltd, Tokyo, Japan), respectively, in quartz cells of 1 cm path length at 20 ± 1 °C. Ultraviolet thermal melting studies were performed on a Shimadzu UV260 spectrophotometer equipped with a thermoprogrammer (KPC-5) and temperature controller (SPR-5) in stoppered quartz cuvettes of 1 cm path length, monitoring the absorbance change at the absorption maximum of the polymer.

### 5.3. Analysis of binding data

Results from absorbance and fluorimetric titration were cast into the form of Scatchard plots of $r/C_f$ versus $r$, in the case of EB, MB, and BER, where $r$ is the number of molecules of ligand bound per mole of nucleotide and $C_f$ is the molar concentration of the free ligand. The parameters $r$ and $C_f$ were determined from the change in absorbance or fluorescence emission intensity. If $A_F(I_F)$, $A_B(I_B)$, and $A(I)$ represent, respectively, the absorbance (or fluorescence) of the initially, finally, and partially titrated ligands, then the fraction of the bound ligand molecules $\alpha_b$ would be given by

$$\alpha_b = A_F(I_F) - A(I)/A_F(I_F) - A_B(I_B) \quad (1)$$

The molar concentration of free ($C_f$) and bound ($C_b$) ligand molecules and $r$ could be evaluated from the following equations where $D$ and $P$ represent the total input ligand and DNA phosphate concentrations, respectively.

$$\begin{aligned} C_f &= (1 - \alpha_b)D \\ C_b &= \alpha_b D \\ r &= C_b/P = \alpha_b D/P \end{aligned} \quad (2)$$

Non-linear binding isotherms were observed in each case and the data were further fitted to a theoretical curve drawn for non-linear non-cooperative ligand binding phenomena using McGhee and von Hippel equation

$$r/C_f = K(1 - nr)[(1 - nr)/\{1 - (n - 1)r\}]^{(n-1)} \quad (3)$$

where '$K$' is the intrinsic binding constant to an isolated binding site and '$n$' is the number of nucleotides occluded by the binding of a single ligand molecule. Binding data were analyzed using the computer program SCATPLOT[35] version 1.2 that works on an algorithm that determines the best-fit parameters to Eq. 3 as described earlier.[75]

### 5.4. Fluorescence quantum yield

Steady state fluorescence quantum yield was calculated using the following equation as described previously:[76]

$$\phi_s = (F_s\varepsilon_q C_q/F_q\varepsilon_s C_s)0.55 \quad (4)$$

where $F$ denotes the integral area of the fluorescence in arbitrary units, $\varepsilon$ represents the molar extinction coefficient at the wavelength of excitation, $C$ represents the molar concentration of the sample (s) and quinine sulfate (q), respectively. Quinine sulfate in 0.1 N $H_2SO_4$ was taken as reference standard for quantum yield measurements.

### 5.5. Fluorescence polarization anisotropy

Fluorescence polarization anisotropy of a ligand and its complexes with A-form or protonated form RNA was carried out as described by Larsson et al.[77]

$$A = (I_{vv} - I_{vh}G)/(I_{vv} + 2I_{vh}G) \quad (5)$$

where $G$ is the ratio $I_{hv}/I_{hh}$ used for instrumental correction. $I_{vv}$, $I_{vh}$, $I_{hv}$, and $I_{hh}$ represent the fluorescence signal for excitation and emission with the polarizer set at (0°,0°), (0°,90°), (90°,0°) and (90°,90°) respectively. The molecular weight of ribonucleic acid used in the study was in the range of 260 ± 50 base pairs.

### 5.6. Circular dichroism

Circular dichroic (CD) spectra were acquired on a JASCO J720 spectropolarimeter (Japan Spectroscopic Co. Ltd, Japan) at 20 ± 1 °C as described previously.[78,79] Titrations were carried out keeping a fixed concentration of the RNA and incrementally adding aliquots of the drugs in 1 cm path length cell. In practice, samples were equilibrated for at least 5 min before the initiation of the spectral accumulations. Each spectrum was the average of four successive accumulations, and was base line corrected and smoothed within permissible limits using builtin software. The spectra presented are normalized to nucleotide concentration and the molar ellipticity ($\theta$) is expressed in deg cm$^2$/dmol.

### 5.7. Solution viscosity measurements

Viscosity experiments were conducted using a Cannon–Manning semi-micro size 75 capillary viscometer that was immersed in a thermostated bath (Cannon Instruments Co., State College, PA, USA) maintained at 20 ± 0.5 °C. RNA duplexes were sonicated to an average molecular weight of 260 ± 50 base pairs using a Labsonic 2000 sonicator (B. Braun Swiss) with a needle probe of 4 mm diameter as describer earlier.[80] After sonication, the polymer was extensively dialyzed under sterile conditions. Flow times were measured in triplicate to an accuracy of ±0.01 s with an electronic stopwatch Casio Model HS-30W (Casio Computer Co. Ltd, Japan). Relative viscosities for RNA in either the presence or absence of the drugs were calculated from the relation

$$\eta'_{sp}/\eta_{sp} = \{(t_{complex} - t_o)/t_o\}/\{(t_{control} - t_o)/t_o\} \quad (6)$$

where $\eta'_{sp}$ and $\eta_{sp}$ are specific viscosities of the alkaloid–RNA complex and the RNA, respectively, $t_{complex}$, $t_{control}$, and $t_o$ are the average flow times for the RNA–drug complex, free RNA, and buffer, respectively. The relative increase in length $L/L_o$ can be obtained from a

corresponding increase in relative viscosity with the use of the following equation:[81]

$$L/L_o = (\eta/\eta_o)^{1/3} = 1 + \beta r \quad (7)$$

where $L$ and $L_o$ are the contour lengths of RNA in presence and absence of the ligands, and $\eta$ and $\eta_o$ are the corresponding values of intrinsic viscosity (approximated by the reduced viscosity $\eta = \eta_{sp}/C$ where $C$ is the RNA concentration) and $\beta$ is the slope when $L/L_o$ is plotted against $r$.

## Acknowledgments

Dr. Rangana Sinha is a Research Associate of the Council of Scientific and Industrial Research (CSIR), Govt. of India. Md. Maidul Islam, Kakali Bhadra, and Anamika Banerjee were supported by Junior Research fellowships (NET) of CSIR.

## References and notes

1. Wilson, W. D. In *Comprehensive Natural Products Chemistry*; Elsevier Science: New York, 1997; Vol. 7.
2. Geierstanger, B. H.; Wenmer, D. E. Annual Review of Biophysics and Biomolecular Structure Annual Reviews, Palo Alto, 463, 1995.
3. Waring, M. J. *Annu. Rev Biochem.* **1981**, *50*, 159.
4. Dervan, P. B. *Bioorg. Med. Chem.* **2001**, *9*, 2215.
5. Wilson, W. D.; Jones, R. L. In *Intercalation Chemistry*; Academic Press: NY, 1982, p 445.
6. Chaires, J. B. *Curr. Opin. Struct. Biol.* **1998**, *8*, 314.
7. Zimmer, C. *Prog. Nucleic Acids Res. Mol. Biol.* **1975**, *15*, 285.
8. Zimmer, C.; Wahnert, U. *Prog. Biophys. Mol. Biol.* **1986**, *47*, 31.
9. Gallego, J.; Varani, G. *Acc. Chem. Res.* **2001**, *34*, 836.
10. Conn, G. L.; Draper, D. E. *Curr. Opin. Struct. Biol.* **1998**, *8*, 278.
11. Afshar, M.; Prescot, C. D.; Varani, G. *Curr. Opin. Biotechnol.* **1999**, *10*, 59.
12. Zapp, M. L.; Young, D. W.; Kumar, A.; Singh, R.; Boykin, D. W.; Wilson, W. D.; Green, M. R. *Bioorg. Med. Chem.* **1997**, *5*, 1149.
13. Hermann, T.; Westhof, E. *J. Mol. Biol.* **1998**, *276*, 903.
14. Wang, Y.; Rando, R. R. *Chem. Biol.* **1995**, *2*, 281.
15. Wilson, W. D.; Ratmeyor, L.; Zhao, M.; Strekowski, L.; Boykin, D. *Biochemistry* **1993**, *32*, 4098.
16. Mc Connaughie, A. W.; Spychala, J.; Zhao, M.; Boykin, D.; Wilson, W. D. *J. Med. Chem.* **1994**, *37*, 1063.
17. Tanious, F. A.; Veal, J. M.; Buczak, H.; Ratmeyer, L. S.; Wilson, W. D. *Biochemistry* **1992**, *31*, 3103.
18. Zhao, M.; Janda, L.; Nguyen, J.; Strekowski, L.; Wilson, W. D. *Biopolymers* **1994**, *34*, 61.
19. Babayan, Y.; Manzini, G.; Xodo, L. E.; Quadrifoglio, F. *Nucleic Acids Res.* **1987**, *15*, 5803.
20. Bresloff, J. L.; Crothers, D. M. *Biochemistry* **1981**, *20*, 3547.
21. Antony, T.; Atreyi, M.; Rao, M. V. R. *Chem. Biol. Int.* **1995**, *97*, 199.
22. Antony, T.; Atreyi, M.; Rao, M. V. R. *J. Biomol. Struct. Dyn.* **1993**, *11*, 067.
23. Kapuscinski, J.; Darzynkiewicz, Z.; Melamed, M. R. *Cytometry* **1982**, *2*, 201.
24. Kapuscinski, J.; Darzynkiewicz, Z.; Melamed, M. R. *Biochem. Pharmacol.* **1983**, *32*, 3679.
25. Das, S.; Banerjee, A.; Sen, A.; Maiti, M. *Curr. Sci.* **2000**, *79*, 82.
26. Sen, A.; Maiti, M. *Indian J. Biochem. Biophys.* **2002**, *39*, 106.
27. Nandi, R.; Debnath, D.; Maiti, M. *Biochim. Biophys. Acta* **1990**, *1049*, 339.
28. Yadav, R. C.; Kumar, G. S.; Bhadra, K.; Giri, P.; Sinha, R.; Pal, S.; Maiti, M. *Bioorg. Med. Chem.* **2005**, *13*, 165.
29. Schlstedt, U.; Aich, P.; Bergman, J.; Vallberg, H.; Norden, B.; Graslund, A. *J. Mol. Biol.* **1998**, *278*, 31.
30. Manzini, G.; Xodo, L.; Barcellona, M. L.; Quadrifoglio, F. *Nucleic Acids Res.* **1985**, *13*, 8955.
31. Dassonneville, L.; Hamy, F.; Colson, P.; Houssier, C.; Bailly, C. *Nucleic Acids Res.* **1997**, *25*, 4487.
32. Pilch, D. S.; Kirolos, M. A.; Liu, X.; Plum, G. E.; Breslauer, K. *J. Biochem.* **1995**, *34*, 9962.
33. Helene, C.; Toulme, J.-J. *Biochim. Biophys. Acta* **1990**, *1049*, 99.
34. McGhee, J. D.; von Hippel, P. H. *J. Mol. Biol.* **1974**, *86*, 469.
35. Ray, A.; Maiti, M.; Nandy, A. *Comput. Biol. Med.* **1996**, *26*, 497.
36. Zimmer, C.; Luck, G.; Venner, H.; Fric, J. *Biopolymers* **1968**, *6*, 563.
37. Guschlbauer, W.; Courtois, Y. *FEBS Lett.* **1968**, *1*, 183.
38. Robinson, H.; van der Marel, G. A.; van Boom, J. H.; Wang, A. H. *J. Biochemistry* **1992**, *31*, 10510.
39. Topping, R. J.; Stone, M. P.; Brush, C. K.; Harris, T. M. *Biochemistry* **1988**, *27*, 7216.
40. Kumar, G. S.; Maiti, M. *J. Biomol. Struct. Dyn.* **1994**, *12*, 183.
41. Kumar, G. S.; Das, S.; Bhadra, K.; Maiti, M. *Bioorg. Med. Chem.* **2003**, *11*, 4861.
42. Bhadra, K.; Kumar, G. S.; Das, S.; Islam, Md. M.; Maiti, M. *Bioorg. Med. Chem.* **2005**, *13*, 4851.
43. Patel, D. J.; Bouaziz, S.; Kettani, A.; Wang, Y. In *Oxford Hand Book of Nucleic Acid Structure*; Neidle, S., Ed.; Oxford University Press, 1999.
44. Thiele, D.; Guschlbauer, W. *Biopolymers* **1971**, *10*, 143.
45. Rich, A.; Davies, D. R.; Crick, F. H.; Watson, J. D. *J. Mol. Biol.* **1961**, *3*, 71.
46. Sarih, L.; Campos, H. E.; Tharand, D.; Litvak, S. *FEBS Lett.* **1980**, *122*, 100.
47. Neidle, S.; Abraham, Z. *CRC. Crit. Rev. Biochem.* **1984**, *17*, 73.
48. Nelson, J. W.; Tinoco, I., Jr. *Biopolymers* **1984**, *23*, 213.
49. Baguley, B. C.; Falkenhaug, E. M. *Nucleic Acids Res.* **1978**, *5*, 161.
50. Aktipis, S.; Kindelis, A. *Biochemistry* **1973**, *12*, 1213.
51. Gatti, C. C.; Houssier, C.; Fredericq, E. *Biochim. Biophys. Acta* **1975**, *407*, 308.
52. Hardin, C. C.; Walker, G. T.; Tinoco, I., Jr. *Biochemistry* **1988**, *27*, 4178.
53. Walker, G. T.; Stone, M. P.; Krug, T. R. *Biochemistry* **1985**, *24*, 7462.
54. Das, S.; Kumar, G. S.; Maiti, M. *Biophys. Chem.* **1999**, *76*, 199.
55. Yang, X. L.; Wang, A. H.J. *Pharmacol. Ther.* **1999**, *83*, 181.
56. Wadkins, R. M.; Jares-Erijman, E. A.; Klement, R.; Rudiger, A.; Jovin, T. M. *J. Mol. Biol.* **1996**, *262*, 53.
57. Mohr, H.; Knuver-Hopf, J.; Lambrecht, B.; Scheidecker, H.; Schmitt, H. *Ann. Hematol.* **1992**, *65*, 224.
58. van den Besselaar, A. M. H. P.; Moor, A. C. E. *J. Clin. Pathol.* **2000**, *53*, 470.

59. Huang, Q.; Fu, W.-L.; Chen, B.; Huang, J.-F.; Zhang, X.; Xue, Q. *J. Photochem. Photobiol. B. Biol.* **2004**, *77*, 39.
60. Atherton, S. J.; Harriman, A. *J. Am. Chem. Soc.* **1993**, *115*, 1816.
61. Hagmar, P.; Pierrou, S.; Nielsen, P.; Norden, B.; Kubista, M. *J. Biomol. Struct. Dyn.* **1992**, *9*, 667.
62. Dardare, N.; Platz, M. S. *Photochem. Photobiol.* **2002**, *75*, 561.
63. Murthy, M. R. V.; Malhotra, L. C. In *Protein Dye interactions Developments and Applications*; Elsevier Applied Science: Amsterdam, 1989, p 316.
64. Kelly, J. M.; van der Putten, W. J.; McConnell, D. J. *Photochem. Photobiol.* **1987**, *45*, 167.
65. Liu, Z. R.; Wilkie, A. M.; Clemens, M. J.; Smith, C. W. *RNA* **1996**, *2*, 611.
66. Debnath, D.; Kumar, G. S.; Nandi, R.; Maiti, M. *Indian J. Biochem. Biophys.* **1989**, *26*, 201.
67. Debnath, D.; Kumar, G. S.; Maiti, M. *J. Biomol. Struct. Dyn.* **1991**, *9*, 061.
68. Coll, M.; Frederick, C. A.; Wang, A. H. J.; Rich, A. *Proc. Natl. Acad. Sci. U.S.A.* **1987**, *84*, 8385.
69. Mischiati, C.; Finotti, A.; Sereni, A.; Boschetti, S.; Baraldi, P. G.; Romagnoli, R.; Feriotto, G.; Jeang, K. T.; Bianchi, N.; Borgatti, M.; Gambari, R. *Biochem. Pharmacol.* **2004**, *67*, 401.
70. Minchenkova, L.; Zimmer, C. *Biopolymers* **1980**, *19*, 823.
71. Bailly, C.; O'Huigin, C.; Houssin, R.; Colson, P.; Houssier, C.; Rivalle, C.; Bisagni, E.; Henichart, J. P.; Waring, M. J. *Mol. Pharmacol.* **1992**, *41*, 845.
72. Bailly, C.; Colson, P.; Houssier, C.; Hamy, F. *Nucleic Acids Res.* **1996**, *24*, 1460.
73. Saenger, W. *Principles of Nucleic acid Structure*; Springer: New York, 1984.
74. Neidle, S. In *Landolt-Bornstein*, Vol III/1b, *Nucleic Acids*; Saenger, W., Ed.; Springer: Heidelberg, 1989; p 247.
75. Nandi, R.; Chakraborty, S.; Maiti, M. *Biochemistry* **1991**, *30*, 3715.
76. Maiti, M.; Nandi, R.; Chaudhury, K. *Photochem. Photobiol.* **1983**, *38*, 245.
77. Larsson, A.; Carlsson, C.; Jonsson, M.; Albinsson, B. *J. Am. Chem. Soc.* **1994**, *116*, 8459.
78. Ray, A.; Maiti, M. *Biochemistry* **1996**, *35*, 7394.
79. Ray, A.; Kumar, G. S.; Das, S.; Maiti, M. *Biochemistry* **1999**, *38*, 6239.
80. Maiti, M.; Nandi, R.; Chaudhuri, K. *FEBS Lett.* **1982**, *142*, 280.
81. Muller, W.; Crothers, D. M. *J. Mol. Biol.* **1968**, *35*, 252.